11 Interpreting Observations

11.1 INTRODUCTORY REMARKS

To describe the flow of a particular glacier, the appropriate model needs to be selected first. In some instances, the choice is obvious. For example, the lamellar flow model discussed in Section 4.2 is based on the assumption that the driving stress is balanced by drag at the glacier base. For floating ice shelves, basal drag is zero and the lamellar flow model does not apply. Most often, the choice is less clear. For example, many of the West Antarctic ice shelves have formed in embayments, and lateral drag may provide much, if not all, of the resistance to flow. It is not immediately obvious whether the ice-shelf model described in Section 4.5 applies best or whether the lateral-drag model of Section 4.4 should be used. On the Siple Coast ice streams, the concave surface profile has led some authors to propose that the flow along these drainage routes is primarily controlled by gradients in longitudinal stress and that other resistive stresses may be neglected when modeling these ice streams. Because the selected model determines to a large extent the predicted behavior of the glacier under consideration, it is important to include the major sources of flow resistance. To be on the safe side, one could use a complete model in which all stresses are calculated at depth. Increasingly, higher-order full-Stokes models are being applied to model glacier flow, but this may not always be a very practical solution, especially when trying to model the evolution of an ice sheet over an extended period of time. Therefore, one often seeks simpler models that realistically include the most important physical processes, treating the less important processes in a parameterized way. This means that the relative importance of the potential sources of resistance to flow needs to be known.

The essential difference between the models described in Chapter 4 is the source of flow resistance. In the lamellar flow model (Section 4.2), basal drag provides the sole resistance, while in the lateral drag model (Section 4.4), drag at the glacier sides is the controlling resistance. On free-floating ice shelves, only gradients in longitudinal stress oppose the driving stress (Section 4.5). Selecting any of these models to describe a certain glacier requires at least some data such as measured surface velocities and surface slopes to evaluate whether the model applies to the glacier being modeled. Too often, modelers develop models that are based mostly on limitations imposed by numerical or analytical techniques, with justification provided by "physical intuition." There is nothing wrong with developing hypothetical models, but claims that such models apply to actual glaciers or ice sheets when measurements indicate otherwise reveal more about the modeler than the model reveals about the glacier.

The force-budget technique discussed in Chapter 3 was developed to determine the mechanical controls on a glacier. The basic equations express balance

of forces, stating that the driving stress is balanced by resistance to flow from gradients in longitudinal stress, lateral drag, and basal drag. The driving stress is estimated from glacier geometry, while the terms involving gradients of the resistive stresses are estimated from measured surface velocities. Basal drag is estimated from the requirement that the sum of all forces acting on a section of glacier must be zero. Taking the x-axis in the average direction of flow, force balance in this direction is

$$\tau_{dx} = \tau_{bx} - \frac{\partial}{\partial x}(H\bar{R}_{xx}) - \frac{\partial}{\partial y}(H\bar{R}_{xy}). \tag{11.1}$$

A similar equation applies to force balance in the second horizontal direction.

Equation (11.1) applies to the full ice thickness, and the resistive stresses in this equation are the depth-averaged stretching stress and lateral shear stress. It is possible to extend the force balance to calculate velocities, strain rates, and stresses at depth, as was done by Whillans et al. (1989) for Byrd Glacier in East Antarctica. The solution scheme is described in Van der Veen (1989; 1999b, Sections 3.4 and 3.5), but for most applications, it is sufficient to consider depth-averaged force balance. This so-called isothermal block-flow model has the great merit of being simple to carry out. Its drawback is that the viscous terms in the balance equations (the last two terms in equation (11.1)) tend to be overestimated because surface values of velocity and strain rates are applied to the entire glacier thickness. Thus, the inferred value for basal drag represents a limiting value. The other extreme value for basal drag can be found by setting the viscous terms equal to zero, that is, by equating basal drag to the driving stress. The actual value for basal drag may be expected to fall in between these two extremes.

Section 11.2 discusses application of the isothermal block-flow model to Byrd Glacier, updating the earlier results of Whillans et al. (1989). These calculations are best performed on regularly spaced data. To minimize errors introduced by measurement uncertainty and small-scale variations in velocity and surface elevation, the horizontal grid spacing should be on the order of one to two ice thicknesses so that derivatives are calculated over distances of two to four ice thicknesses. For Byrd Glacier, which is ~25 km wide, this gives enough spatial resolution to estimate lateral drag across the glacier. For narrow glaciers, this approach is not well suited. For example, the fast-moving part of Jakobshavn Isbræ in West Greenland is only 2 to 4 km wide. With a thickness of ~1 km, an appropriate grid spacing would be 1 to 2 km, which would give one or two gridpoints across the glacier. Clearly, this is insufficient to find a meaningful estimate for lateral drag. Decreasing the grid spacing would increase uncertainties in calculated force-balance terms. Therefore, for narrow glaciers, a two-step approach to evaluating force balance is proposed. First, the role of gradients in longitudinal stress in opposing the driving stress is estimated by considering flow along the central flowline as described in Section 11.3. Next, transects of velocity across the glacier are used to evaluate lateral drag at regular intervals along the glacier (Section 11.4). By combining the results from both calculations, basal drag can be estimated.

The force-balance technique is a diagnostic tool to investigate location and magnitude of resistance to flow on glaciers. By conducting calculations for successive time periods, changes in resistive forces can be evaluated, as was done by Van der Veen et al. (2011) for a 10-year period during which Jakobshavn Isbræ underwent large changes. While determining *how* partitioning of flow resistance is a necessary first step, it does not necessarily provide an answer to the question of *why* this partitioning changed.

11.2 LOCATING MECHANICAL CONTROLS

To illustrate the steps involved in the force-budget technique, application of the isothermal block-flow model to Byrd Glacier is considered. Byrd Glacier is one of the major outlet glaciers of the East Antarctic Ice Sheet, draining through the Transantarctic Mountains into the Ross Ice Shelf. Figure 11.1 shows the geometry of the lower reach of the glacier. The surface elevation is derived from ASTER (Advanced Spaceborne Thermal Emission and Reflection Radiometer) satellite imagery (Stearns, 2007), while the bed topography was determined from airborne radar sounding conducted in 2011–2012 by the Center for Remote Sensing of Ice Sheets at the University of Kansas (S. P. Gogineni, pers. comm., 2012). The lower panel shows the height above buoyancy, defined as

$$H_{ab} = H + \frac{\rho_w}{\rho} H_b, \tag{11.2}$$

with H the ice thickness (third panel), H_b the bed elevation (second panel; negative when below sea level), and ρ_w and ρ the density of sea water and ice, respectively. On the floating ice shelf, $H_{ab} = 0$, and the zero-contour in this map indicates the position of the grounding line where ice transitions from grounded to floating.

Original point measurements of surface and bed elevation were gridded to obtain values at regular gridpoints in the (x, y) coordinate system, with the x-axis horizontal and mainly downglacier, and the y-axis perpendicular and counterclockwise to the x-axis in map view. In the following, values at gridpoints denoted by two counters, namely, i = 1, 2, …, I for the x-direction and j = 1, 2, …, J for the y-direction, (i, j) = (1, 1) corresponds to the gridpoint in the lower left corner of the maps in Figure 11.1. The grid spacing is 2 km in both horizontal directions.

The first step is to calculate the two components of driving stress, given by

$$\tau_{dx} = -\rho g H \frac{\partial h}{\partial x}, \tag{11.3}$$

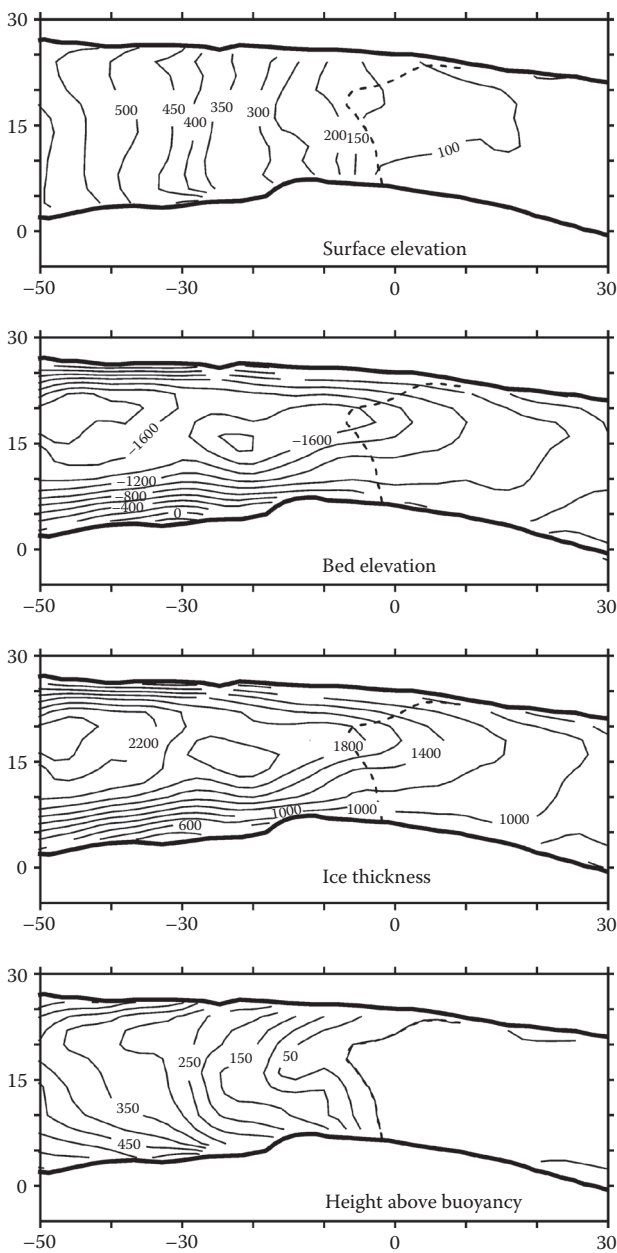$$\tau_{dy} = -\rho g H \frac{\partial h}{\partial y}, \tag{11.4}$$

FIGURE 11.1 Surface elevation (contour interval: 50 m above sea level), bed elevation (contour interval: 200 m above sea level), ice thickness (contour interval: 200 m), and height above buoyancy (contour interval: 50 m) on Byrd Glacier. Ice flow is from left to right. The dashed line represents the grounding line as determined from the flotation criterion. Glacier data in this and the following figures have been transferred to a local coordinate system oriented such that ice flow is predominantly in the x-direction.
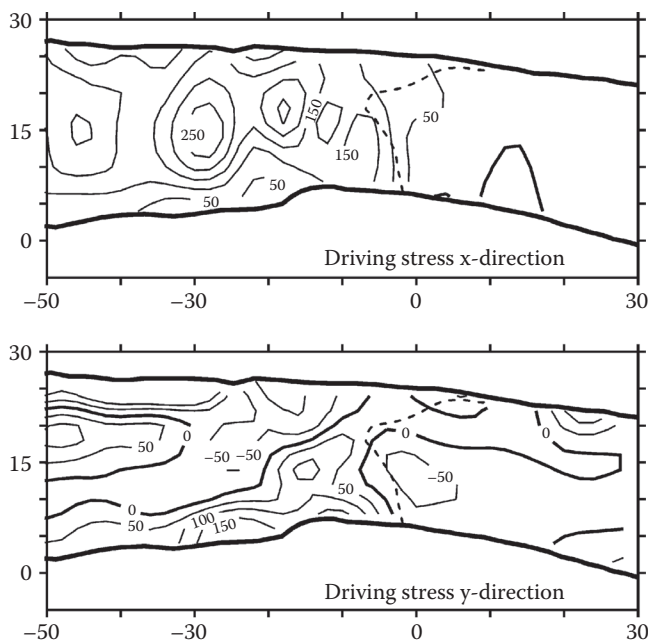
FIGURE 11.2   Two components of the driving stress on Byrd Glacier (contour interval: 50 kPa).

in which h represents the elevation of the ice surface. With values of H and h known at gridpoints (i, j), the two components of driving stress can be estimated at grid-points using central differencing, and

$$\tau_{dx}(i, j) = -\rho g H(i, j) \frac{h(i+1, j) - h(i-1, j)}{2 \Delta x}, \tag{11.5}$$

$$\tau_{dy}(i, j) = -\rho g H(i, j) \frac{h(i, j+1) - h(i, j-1)}{2 \Delta y}, \tag{11.6}$$

where $\Delta x = \Delta y$ represents the spacing between neighboring gridpoints. Figure 11.2 shows values of the two components of driving stress. Values of the driving stress are small on the ice shelf and larger and more variable on the grounded portion. While the flow of the glacier is approximately in the x-direction, there is a significant component of driving stress in the transverse direction. This component is associated with longitudinal flow stripes on the glacier.

The next step is to calculate surface strain rates from measured surface veloc-ities. These velocities are derived from feature tracking on two ASTER satellite images (12/5/2005–1/28/2007; Stearns, 2007). The two components of the velocity in the local coordinate system are shown in Figure 11.3. Greatest speeds are near the
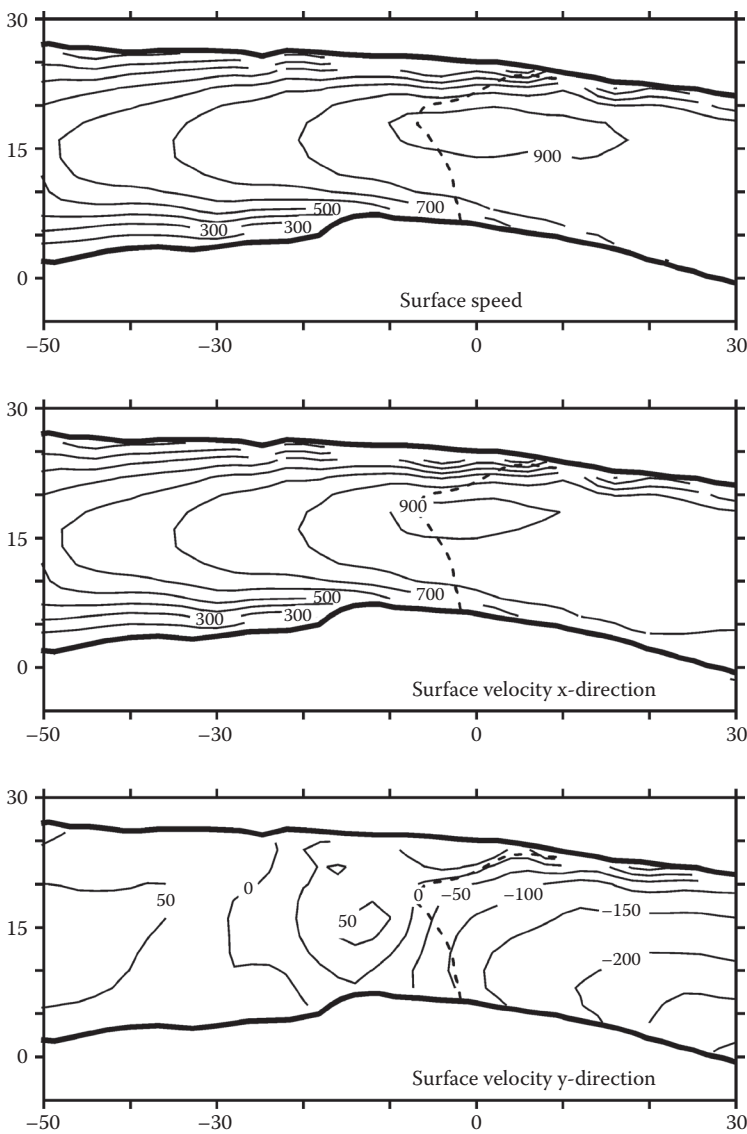
FIGURE 11.3 Measured surface velocity on Byrd Glacier (contour interval: 100 m/yr in the upper two panels, 50 m/yr in the lower panel).

grounding line and in the center of the glacier. The velocity decreases to zero at the lateral margins.

Because depth-averaged flow is considered, only three strain rate components need to be considered, namely, longitudinal stretching or compression, $\dot{\varepsilon}_{xx}$, transverse stretching or compression, $\dot{\varepsilon}_{yy}$, and shearing, $\dot{\varepsilon}_{xy}$. From the definitions given in Section 1.2, these strain rates are linked to velocity gradients. Denoting the velocity

in the x-direction by U and that in the y-direction by V, applying finite differencing to equation (1.34) allows the strain rates to be estimated from the following expressions:

$$\dot{\varepsilon}_{xx}(i,j) = \frac{\partial U}{\partial x}(i,j) = \frac{U(i+1,j) - U(i-1,j)}{2\Delta x}, \tag{11.7}$$

$$\dot{\varepsilon}_{yy}(i,j) = \frac{\partial V}{\partial y}(i,j) = \frac{V(i,j+1) - V(i,j-1)}{2\Delta y}, \tag{11.8}$$

$$\dot{\varepsilon}_{xy}(i,j) = \frac{1}{2}\frac{\partial U}{\partial y}(i,j) + \frac{1}{2}\frac{\partial V}{\partial x}(i,j) = \frac{1}{2}\frac{U(i,j+1) - U(i,j-1)}{2\Delta x} + \frac{1}{2}\frac{V(i+1,j) - V(i-1,j)}{2\Delta x}. \tag{11.9}$$

Calculated strain rates are shown in Figure 11.4. The lower panel shows the effective strain rate, defined as

$$2\dot{\varepsilon}_e^2 = \dot{\varepsilon}_{xx}^2 + \dot{\varepsilon}_{yy}^2 + \dot{\varepsilon}_{zz}^2 + 2\left(\dot{\varepsilon}_{xy}^2 + \dot{\varepsilon}_{xz}^2 + \dot{\varepsilon}_{yz}^2\right). \tag{11.10}$$

For the present case, vertical shearing is neglected, while the vertical strain rate, $\dot{\varepsilon}_{zz}$, follows from the incompressibility condition. The effective strain rate then reduces to

$$\dot{\varepsilon}_e^2 = \dot{\varepsilon}_{xx}^2 + \dot{\varepsilon}_{yy}^2 + \dot{\varepsilon}_{xx}\dot{\varepsilon}_{yy} + \dot{\varepsilon}_{xy}^2. \tag{11.11}$$

Invoking the flow law (3.47) and (3.48), the resistive stresses are calculated from strain rates as

$$R_{xx} = B\dot{\varepsilon}_e^{1/n-1}(2\dot{\varepsilon}_{xx} + \dot{\varepsilon}_{yy}), \tag{11.12}$$

$$R_{yy} = B\dot{\varepsilon}_e^{1/n-1}(\dot{\varepsilon}_{xx} + 2\dot{\varepsilon}_{yy}), \tag{11.13}$$

$$R_{xy} = B\dot{\varepsilon}_e^{1/n-1}\dot{\varepsilon}_{xy}. \tag{11.14}$$

Applying these relations yields the surface values for the resistive stresses R_{xx} and R_{xy}, shown in Figure 11.5. Longitudinal tension (upper panel) is generally positive. The ice-shelf portion (beyond x = 0 km) is under about 100 kPa tension. In the grounded portion, this quantity is more variable and locally reaches 250 kPa. Side shear (lower panel) is largest near the lateral margins of the glacier, as expected. Where the glacier is grounded, side shear varies in a complex way across the glacier, but for the ice-shelf portion it decays within about 7 km of the margin and is near zero in the middle portion.

In the balance of forces, gradients in resistive stresses are important (see Section 3.2), and the next step is to use horizontal gradients in the resistive stresses shown in
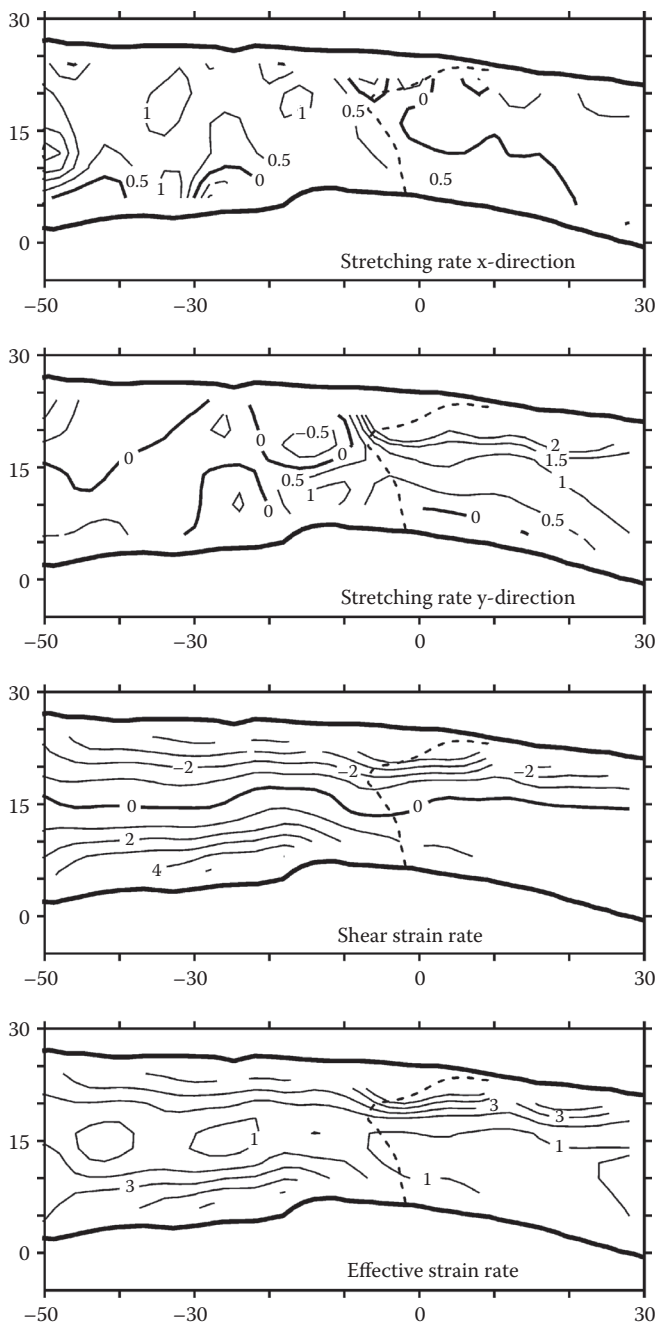
FIGURE 11.4 Derived surface strain rates on Byrd Glacier (contour interval: 0.5×10^{-3} yr^{-1} in the upper two panels, 1×10^{-3} yr^{-1} in the lower two panels).
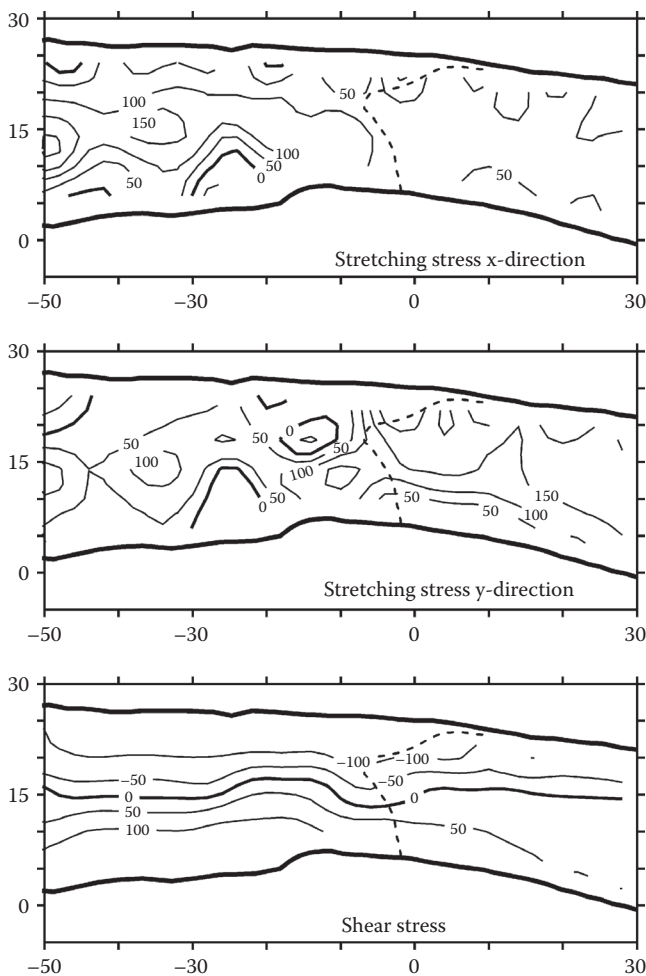
FIGURE 11.5 Resistive stresses on Byrd Glacier (contour interval: 50 kPa).

Figure 11.5 to estimate resistance to flow from longitudinal stress gradients and from lateral drag. First, gradients in longitudinal stress at gridpoints (i, j) are calculated from

$$\frac{\partial}{\partial x}(HR_{xx})(i, j) = \frac{H(i+1, j)R_{xx}(i+1, j) - H(i-1, j)R_{xx}(i-1, j)}{2\,\Delta x}. \qquad (11.15)$$

Lateral drag is calculated from

$$\frac{\partial}{\partial y}(HR_{xy})(i, j) = \frac{H(i, j+1)R_{xy}(i, j+1) - H(i, j-1)R_{xy}(i, j-1)}{2\,\Delta y}. \qquad (11.16)$$

Basal drag can now be calculated from the force-balance equation

$$\tau_{bx} = \tau_{dx} + \frac{\partial}{\partial x}(HR_{xx}) + \frac{\partial}{\partial y}(HR_{xy}). \tag{11.17}$$

A similar expression applies to the second horizontal direction. In Figure 11.6 the results of the force-budget calculation for the approximate direction of flow are shown. The driving stress is shown in the upper panel. The next two panels show the gradient in longitudinal stress and resistance to flow associated with side drag. Adding the three panels together yields the basal drag (last panel). Comparison of the top and bottom panels shows that fluctuations in driving stress are largely muted by the gradient terms, resulting in smaller variations in basal drag. Nevertheless, basal drag is far from uniform. As expected, it is zero under the floating ice-shelf portion. On the grounded part, basal drag is large and variable and appears to be concentrated at isolated spots ("sticky spots").

Because of the relatively simple geometry of Byrd Glacier, force-balance terms in the x-direction correspond mostly to those in the flow direction and can be inter-preted as such. This need not be the case for glaciers where flow may be turning in the downglacier direction. For such glaciers, a final step is needed to complete the force-balance calculations, namely, rotation to a local flow-following coordinate system.

At each location, the direction of ice flow is given by (Section 1.1)

$$\phi(i, j) = \mathrm{atan}\left(\frac{V(i, j)}{U(i, j)} \right), \tag{11.18}$$

with ϕ defined as the angle between the velocity direction and the x-axis (Figure 1.2). This angle is shown in Figure 11.7 and is small on the grounded part. On the ice shelf, the angle increases as the flow turns clockwise onto the Ross Ice Shelf. This flow direction defines a Cartesian coordinate system with the $\tilde{x}$-direction at each location aligned with the flow at that location, and the $\tilde{y}$-direction perpendicular to the flow direction. Generally, the orientation of the $(\tilde{x}, \tilde{y})$ coordinate system differs at each location on the glacier as the flow direction changes along the glacier. In the following expressions, these flow directions are indicated by subscripts l (along flow) and c (cross flow), respectively. Results for the coordinate transformation are shown only for the floating section of Byrd Glacier.

The driving stress is a vector and rotates according to equations (1.5) and (1.6). The component of driving stress in the (local) flow direction is then

$$\tau_{dl} = \tau_{dx} \cos\phi + \tau_{dy} \sin\phi, \tag{11.19}$$

while the cross-flow component is given by

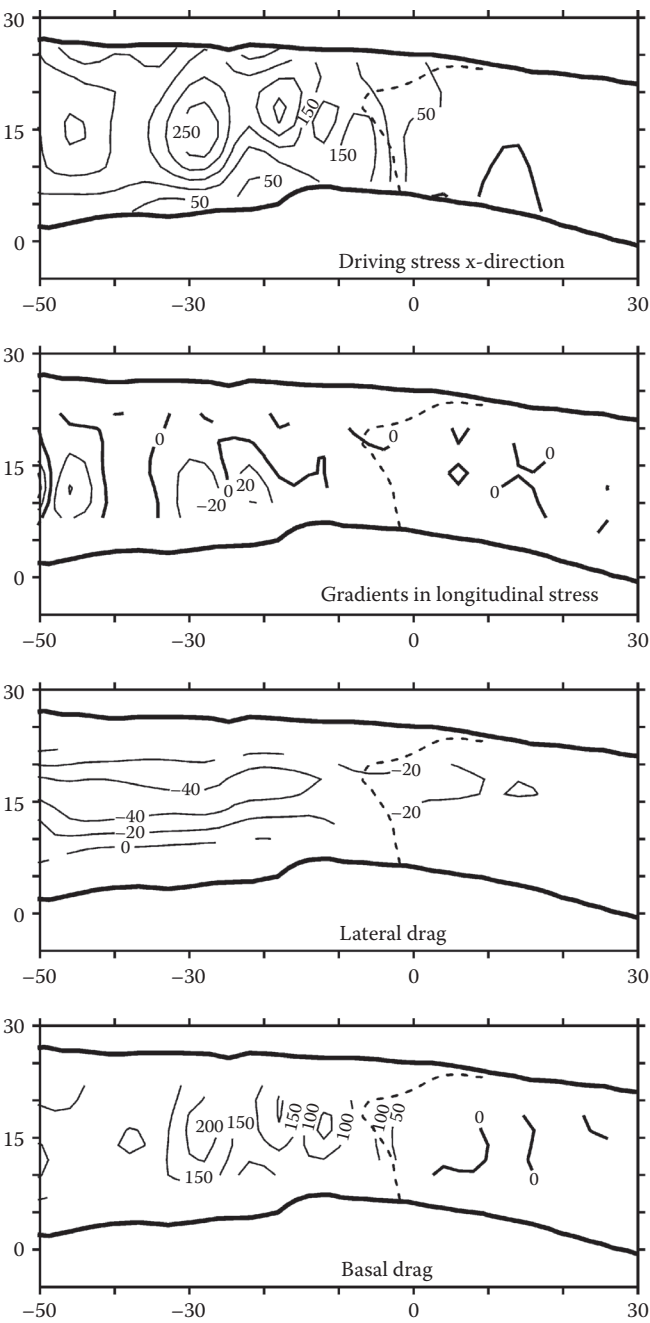$$\tau_{dc} = -\tau_{dx} \sin\phi + \tau_{dy} \cos\phi. \tag{11.20}$$

FIGURE 11.6 Force-balance terms on Byrd Glacier for the x-direction (contour interval: 50 kPa in top and bottom panels, 20 kPa in second and third panels).
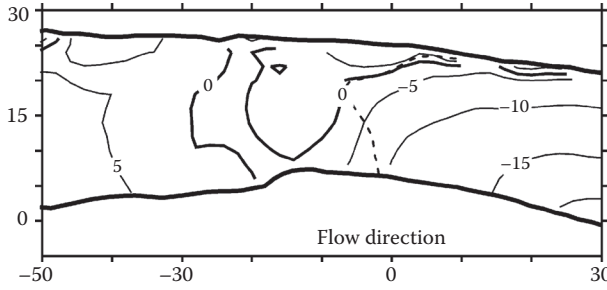
FIGURE 11.7   Angle of flow direction measured relative to the x-direction on Byrd Glacier (contour interval: 5 degrees).

The other terms in the force-balance equation transform similarly. The rotated driving stress is shown in the upper panels of Figure 11.8. For this particular example, there is not much difference between the rotated driving stress components and those in the (x, y) coordinate system because the rotation angle is relatively small.

The three surface strain rates form a 2 × 2 tensor and rotate to the flow-following coordinate system according to (Jaeger, 1969, p. 7; cf. Section 1.1)

$$\dot{\varepsilon}_{ll} = \dot{\varepsilon}_{xx} \cos^2 \phi + \dot{\varepsilon}_{yy} \sin^2 \phi + 2\dot{\varepsilon}_{xy} \sin\phi \cos\phi, \tag{11.21}$$

$$\dot{\varepsilon}_{cc} = \dot{\varepsilon}_{xx} \sin^2 \phi + \dot{\varepsilon}_{yy} \cos^2 \phi - 2\dot{\varepsilon}_{xy} \sin\phi \cos\phi, \tag{11.22}$$

$$\dot{\varepsilon}_{lc} = (\dot{\varepsilon}_{xx} - \dot{\varepsilon}_{yy}) \sin\phi \, \cos\phi + \dot{\varepsilon}_{xy} (\cos^2 \phi - \sin^2 \phi). \tag{11.23}$$

The lower panels in Figure 11.8 compare two of the rotated strain rates to the corresponding strain rates in the (x, y) coordinate system. To find the resistive stresses in the flow-following coordinate system, equations similar to (11.21)–(11.23) are applied.

In addition to estimating the terms in the balance of forces, associated uncertainties should also be estimated. This can be done using the formulas given in Section 1.3 and is not discussed here for the Byrd Glacier example.

11.3   ESTIMATING THE ROLE OF GRADIENTS IN LONGITUDINAL STRESS

The longitudinal resistive stress, R_{xx}, is linked to the along-flow stretching rate or longitudinal gradient in the downstream component of ice velocity through the flow law (3.48). If the dynamic centerline of a glacier is considered, the only nonzero strain rates contributing to the effective strain rate are the along-flow stretching rate and the lateral spreading rate. Along-flow stretching is calculated from the gradient in ice velocity

$$\dot{\varepsilon}_{xx} = \frac{\partial U}{\partial x}, \tag{11.24}$$
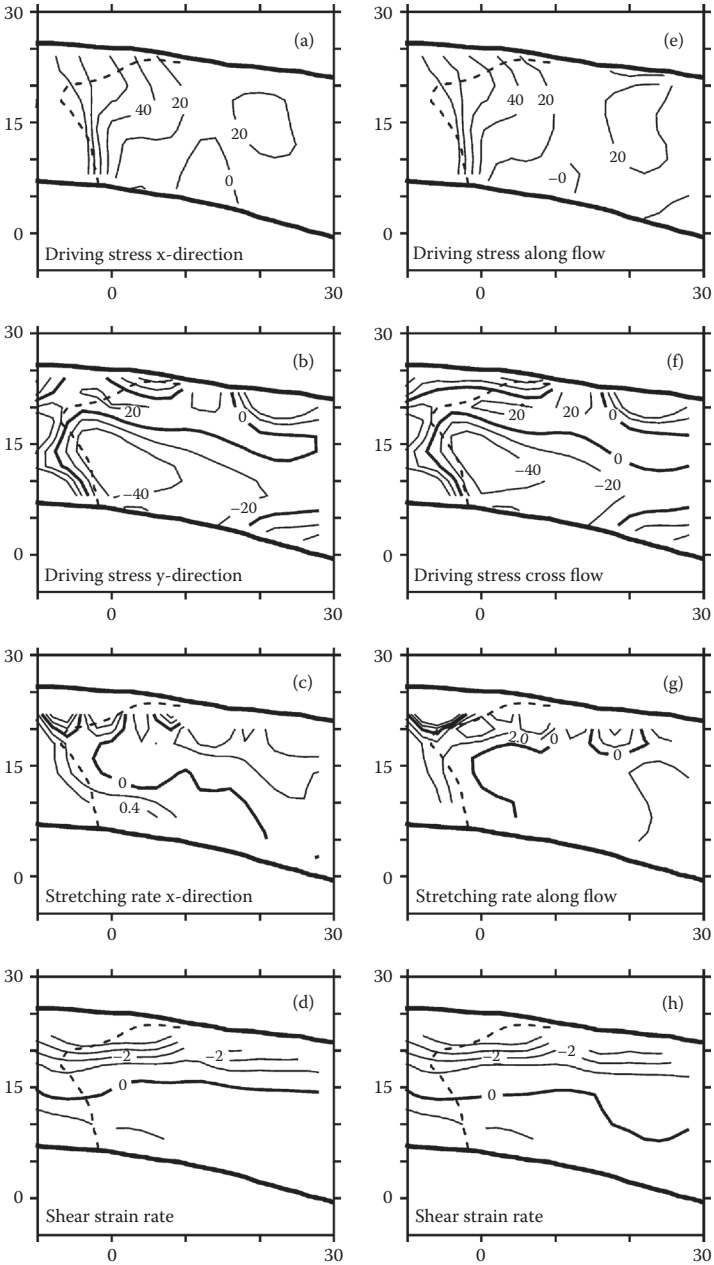
FIGURE 11.8 Two components of driving stress in the original (x, y) coordinate system (panels a and b) and in the flow-following $(\tilde{x}, \tilde{y})$ coordinate system (panels e and f) (contour interval: 20 kPa), and stretching rate and shear strain rate in the original (x, y) coordinate system (panels c and d) and in the flow-following $(\tilde{x}, \tilde{y})$ coordinate system (panels g and h) (contour interval: 0.2×10^{-3} yr^{-1} in panels c and f, and 1.0×10^{-3} yr^{-1} in panels d and h).
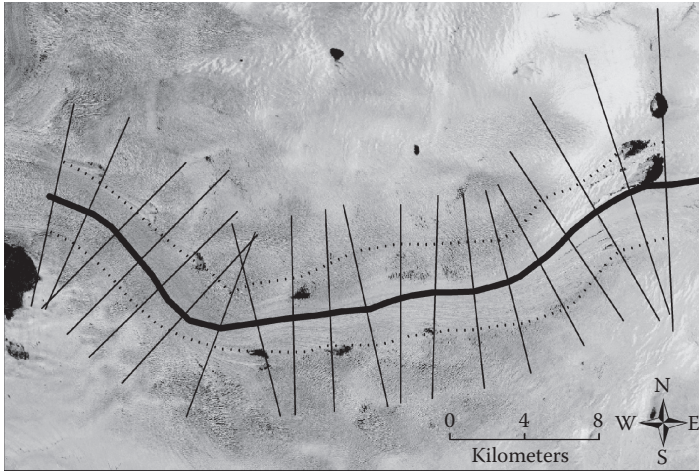
FIGURE 11.9 Map showing the central flowline of the lower 30 km of Jakobshavn Isbræ, and location of velocity transects used to estimate resistance to flow from lateral drag. The dotted lines mark the lateral shear margins. (From Van der Veen, C. J., J. C. Plummer, and L. A. Stearns, *J. Glaciol.,* 57, 770–782, 2011. Reprinted from the *Journal of Glaciology* with permission of the International Glaciological Society and the authors.)

with U the component of velocity in the direction of flow and the x-axis following the flow direction. As shown in Figure 11.9, this axis may be curvilinear as in the case of Jakobshavn Isbræ, West Greenland. Lateral spreading is estimated from the width of the glacier, making the assumption that the ice must remain in contact with the margins. That is,

$$\dot{\varepsilon}_{yy} = \frac{U}{W} \frac{\partial W}{\partial x}. \tag{11.25}$$

This term may be neglected where the glacier width, W, is approximately constant in the flow direction.

On fast-moving outlet glaciers, the contribution to ice discharge from internal deformation is small, and in good approximation, measured surface velocities may be used to estimate the depth-averaged strain rate and resistive stress. Of importance to the balance of forces is how the depth-integrated resistive stress varies along the flowline. That is, resistance to flow from gradients in longitudinal stress is given by

$$F_{lon} = \frac{\partial H R_{xx}}{\partial x}, \tag{11.26}$$

and this term must be compared to the driving stress calculated from the geometry of the glacier to evaluate the importance of longitudinal stress gradients to the flow
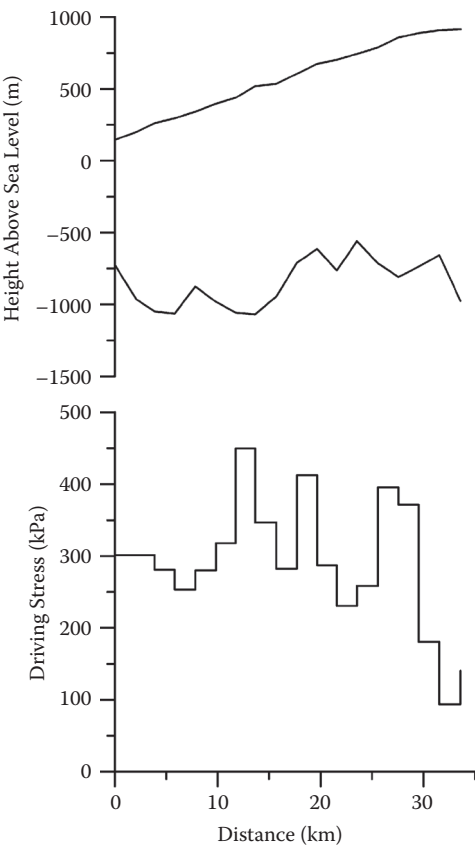
FIGURE 11.10   Surface and bed elevation (2005) along the central flowline of Jakobshavn Isbræ and calculated driving stress. (After Van der Veen, C. J., J. C. Plummer, and L. A. Stearns, *J. Glaciol.,* 57, 770–782, 2011.)

of the glacier. To illustrate the steps involved, results of a calculation for the lower 30 km of Jakobshavn Isbræ are discussed next.

Figure 11.9 shows the central flowline and the lateral boundaries of Jakobshavn Isbræ, as well as across-flow transects used to estimate lateral drag. Section 11.4 discusses how these boundaries were determined and how resistance to flow from lateral drag is estimated. For the present discussion, only the glacier geometry and velocity along the flowline need to be considered. This geometry is shown in the upper panel of Figure 11.10. Surface elevations derive from airborne laser altimetry conducted in 2005, while the bed topography was measured by airborne radar sounding conducted by the Center for Remote Sensing of Ice Sheets at the University of Kansas over multiple years (Gogineni et al., 2001; Van der Veen et al., 2011). From this geometry, the driving stress shown in the lower panel is calculated.

Equally important as calculating the value of the driving stress is to estimate the uncertainty or error in this quantity. This error is estimated using equation (1.40) for propagation of independent errors. Let

$$\alpha = -\frac{\partial h}{\partial x}, \tag{11.27}$$

denote the slope of the ice surface. The driving stress is then given by

$$\tau_{dx} = \rho g H \alpha. \tag{11.28}$$

Neglecting errors in the ice density, ρ, and gravitational constant, g, applying equation (1.40) gives

$$\left(\Delta\tau_{dx}\right)^2 = \rho g \alpha (\Delta H)^2 + \rho g H (\Delta\alpha)^2, \tag{11.29}$$

or

$$\left(\frac{\Delta\tau_{dx}}{\tau_{dx}}\right)^2 = \left(\frac{\Delta H}{H}\right)^2 + \left(\frac{\Delta\alpha}{\alpha}\right)^2. \tag{11.30}$$

The surface slope is calculated as the difference between the surface elevations at two locations, x_1 and x_2, and the uncertainty is given by (compare with equation (1.44))

$$\Delta\alpha = \frac{\Delta h}{x_2 - x_1}\sqrt{2}. \tag{11.31}$$

For the present case, the uncertainty in surface elevation is estimated to be about 0.6 m. Surface slopes are calculated over a nominal distance of 4 km, giving an uncertainty in the slope of $\sim 0.21 \times 10^{-3}$. The uncertainty in ice thickness is ~10 m. With an average ice thickness of 1500 m and an average slope equal to 0.028, the resulting uncertainty in driving stress is

$$\left(\frac{\Delta\tau_{dx}}{\tau_{dx}}\right)^2 = \left(\frac{10}{1500}\right)^2 + \left(\frac{0.21 \times 10^{-3}}{0.028}\right)^2, \tag{11.32}$$

and

$$\frac{\Delta\tau_{dx}}{\tau_{dx}} = 10^{-2}. \tag{11.33}$$

Thus, for this particular example, the error in driving stress is rather small, being about 1% of the value of the driving stress. Because the relative error is so small, error bars are not shown in the lower panel of Figure 11.10.

Next, gradients in longitudinal stress are estimated. The input data for this calculation are surface velocities (Figure 11.11, upper panel) measured from satellite interferometric image pairs collected in October 2005, using standard speckle tracking techniques (Joughin et al., 2008b). Neglecting the contribution of shear strain rates
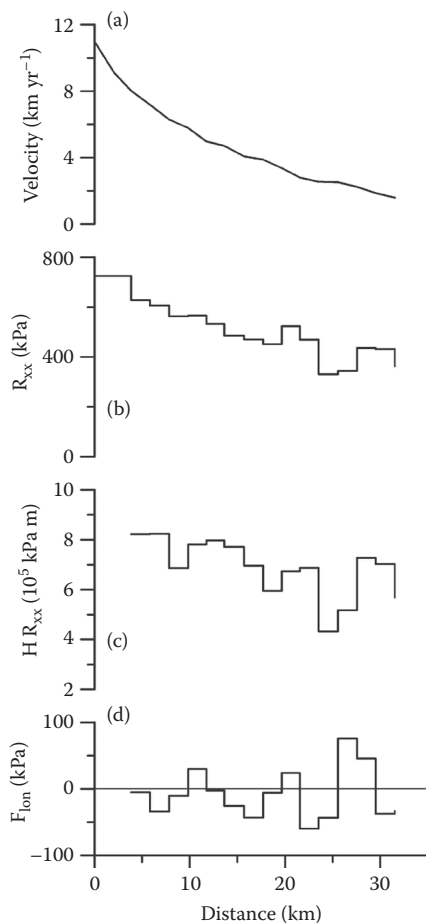
FIGURE 11.11 Steps in the calculation of resistance to flow from gradients in longitudinal stress. Panel a shows the measured surface velocity from which stretching rates (not shown) are calculated. Using the flow law, the corresponding resistive stress (panel b) is calculated. This stress is multiplied by the ice thickness (panel c) and the derivative of this quantity gives F_{lon} (panel d). (After Van der Veen, C. J., J. C. Plummer, and L. A. Stearns, *J. Glaciol.*, 57, 770–782, 2011.)

to the effective strain rate, the longitudinal resistive stress is linked to the stretching rate by invoking the flow law,

$$R_{xx} = 2B\dot{\varepsilon}_{xx}^{1/n}, \tag{11.34}$$

where n = 3 is the flow-law exponent and B the temperature-dependent viscosity parameter. Strain rates are estimated from measured surface velocities and taken to be constant with depth. The value B = 400 kPa $yr^{1/3}$ corresponding to an effective depth-averaged ice temperature of –10°C, is used here. The calculated stretching stress is shown in the second panel in Figure 11.11. The third panel shows gradients

in longitudinal stress multiplied by the ice thickness, as called for in equation (11.25).
Taking the derivative, resistance to flow associated with gradients in longitudinal
stress is obtained. The result is shown in the lower panel in Figure 11.11 and sug-
gests that this term in the balance of forces is small compared to the driving stress.
There are spatial variations in F_{lon}, but it is not clear whether these have an important
effect on the dynamics of the glacier. A linear regression of the curve shown in the
third panel gives an average contribution to the large-scale force balance of ~10 kPa,
compared with an average driving stress of ~250 kPa.

The uncertainty in the calculated force-balance term, F_{lon}, can be estimated using
the expressions given in Section 1.3. For this example, the uncertainty is rather small.

11.4   ESTIMATING RESISTANCE FROM LATERAL DRAG

Resistance from lateral drag is linked to the transverse gradient in lateral shear
(the second term on the right-hand side of the balance equation (11.1)). Thus, where
transects of velocity across a glacier are available, lateral drag can be estimated.
As an example, consider the velocity transect across Jakobshavn Isbræ shown in
Figure 11.12. Following the model described in Section 4.4, the assumption is made
that lateral shearing is the dominant strain rate, so that the lateral shear stress, R_{xy},
can be estimated from equation (4.47). That is

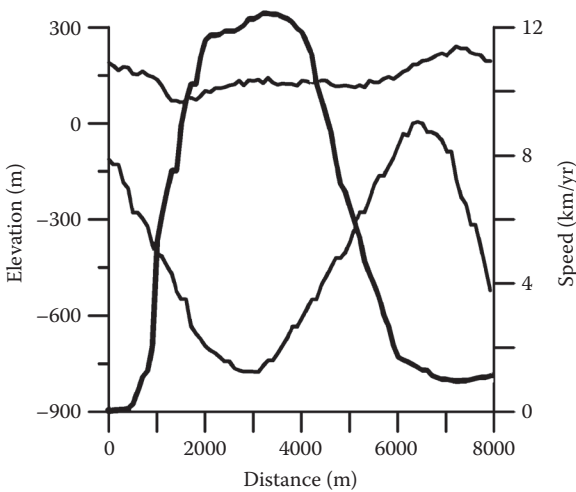$$R_{xy} = B\left(\frac{1}{2}\frac{\partial U}{\partial y}\right)^{1/n},$$ (11.35)

FIGURE 11.12   Surface and bed elevation (scale on the left) and surface velocity (bold curve;
scale on the right) along a transect across Jakobshavn Isbræ. (From Van der Veen, C. J., J. C.
Plummer, and L. A. Stearns, *J. Glaciol.,* 57, 770–782, 2011. Reprinted from the *Journal of
Glaciology* with permission of the International Glaciological Society and the authors.)
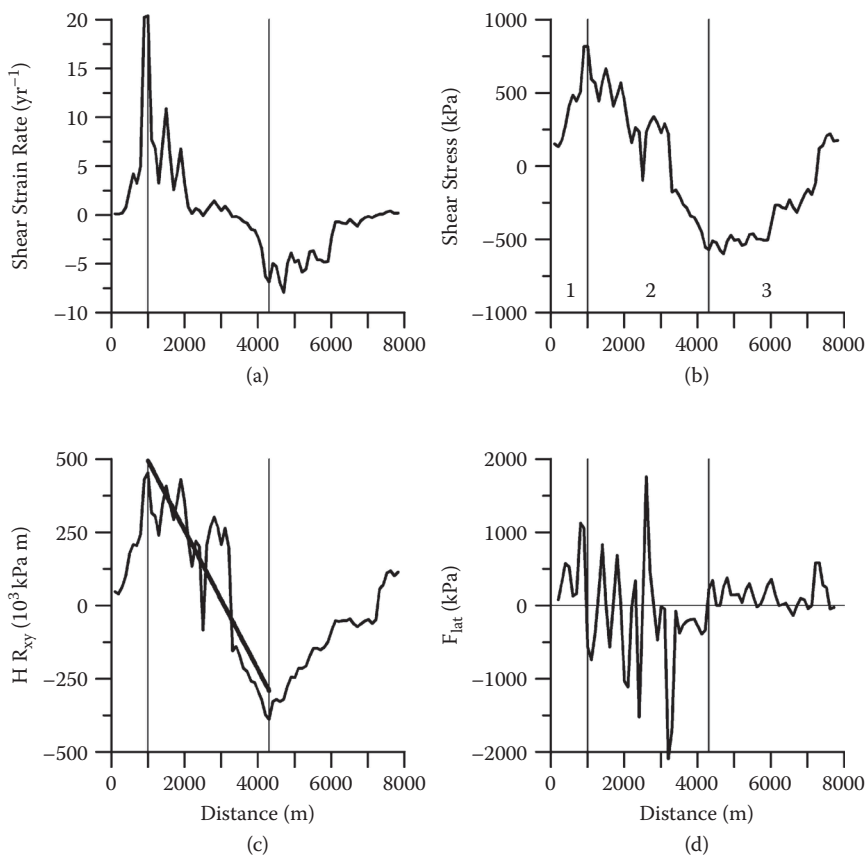
FIGURE 11.13 Steps in the calculation of resistance to flow from lateral drag. Panel a shows the measured surface velocity from which stretching rates (not shown) are calculated. Using the flow law, the corresponding resistive stress (panel b) is calculated. This stress is multiplied by the ice thickness (panel c) and the derivative of this quantity gives F_{lat} (panel d).

where U represents the discharge velocity perpendicular to the transect. This velocity is a function of the transverse distance, y. The corresponding shear strain rate and shear stress are shown in panels a and b of Figure 11.13. Recalling that resistance to flow from lateral drag is given by

$$F_{lat} = -\frac{\partial}{\partial y}(H R_{xy}), \tag{11.36}$$

three different regions can be identified along the transect (panel b): in the central part (region 2), the shear stress decreases in the y-direction and lateral drag opposes the driving stress, while in both outboard regions (1 and 3) the shear stress increases in the y-direction and lateral drag acts in the same way as does the driving stress. Thus, the slower-moving outboard ice is being dragged along by the fast-moving interior

part of the glacier. As a result, basal drag must be greater than the local driving stress in the outboard regions (Whillans and Van der Veen, 1997, 2001; Van der Veen et al., 2007). The minimum and maximum values of lateral shear stress correspond to the two inflection points in the velocity curve shown in Figure 11.12 and define the boundaries of the ice stream (Van der Veen et al., 2011). The vertical lines in Figure 11.13 demarcate the lateral margins of the ice stream at this particular transect.

The curve of lateral shear stress, R_{xy}, shows many small-scale variations that may be associated with small-scale variations in driving stress, or locally important gradients in longitudinal stress. As a result of such variations, applying equation (11.36) to estimate lateral drag across the ice stream typically yields a noisy curve (Figure 11.13, panel d). The main reason why local variability and, to some extent, measurement uncertainties become important when estimating lateral drag is that spatial derivatives in the transverse direction are calculated over relatively short distances. According to equation (1.44), the error in calculated strain rate is inversely proportional to the distance over which the velocity gradient is calculated. When considering along-flow stretching, this distance is typically several tens of km. However, to calculate lateral drag, derivatives are obtained from velocity determinations that are spaced 1 km or less. Thus, for the same uncertainty in velocity, the error in shear strain rate is about 100 times the error in stretching rate. Transverse gradients need to be calculated over much shorter distances because the width of an ice stream or outlet glacier is comparatively small, up to about 30 km for West Antarctic ice streams and only a few km for Jakobshavn Isbræ, compared with a length of up to several hundreds of km. To minimize the uncertainty in calculated lateral drag, the width-averaged balance of forces is considered.

As derived in Section 4.4, the average lateral resistance acting on a section of glacier of unit width can be calculated, using the values of the shear stress, τ_s, at both margins:

$$F_{lat} = \frac{H_1 \tau_{s1} - H_2 \tau_{s2}}{W}. \tag{11.37}$$

In this expression, the subscripts 1 and 2 refer to the southern and northern margin, respectively, and W represents the distance between the two margins. The total width of the transect shown in Figure 11.12 is 3.3 km, while the shear stresses at the margins are 819 kPa and –570 kPa, with corresponding thicknesses of 553 and 683 m, respectively. Substituting these values into equation (11.37) gives F_{lat} = 255 kPa. In other words, averaged over the width of the ice stream, lateral drag supports about 255 kPa of driving stress. Using the formulas for error propagation discussed in Section 1.3, the estimated error in this value is 15 kPa.

Alternatively, F_{lat} can be estimated from linear regression of HR_{xy} against transverse distance, with the regression restricted to the region between the lateral shear margins. The slope of the regression line shown in Figure 11.13c corresponds to a width-averaged lateral drag of 237 kPa with an uncertainty of 23 kPa. Within error limits, both approaches yield the same result.

The relative importance of lateral drag in controlling the flow Jakobshavn Isbræ can now be determined for the entire flowline by comparing F_{lat} calculated for each transect shown in Figure 11.9 to the width-averaged driving stress. This comparison is shown in Figure 11.14 and indicates that over the lower 10 km or so, lateral drag
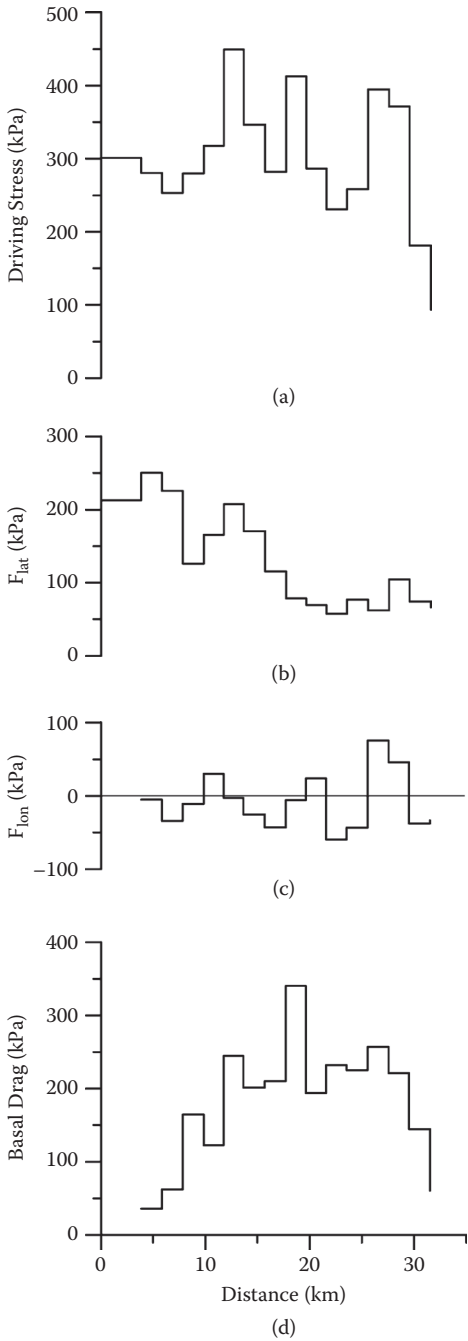
FIGURE 11.14 Force-balance terms along the central flowline of Jakobshavn Isbræ. (After Van der Veen, C. J., J. C. Plummer, and L. A. Stearns, *J. Glaciol.,* 57, 770–782, 2011.)

is the main source of flow resistance. As discussed in Section 11.3, gradients in longitudinal stress are small and contribute little to the balance of forces. Subtracting F_{lat} and F_{lon} from the driving stress yields basal drag (Figure 11.14, panel d). For the upstream part of the flowline, the driving stress is primarily balanced by drag at the glacier base. Toward the glacier front, basal resistance decreases.

Van der Veen et al. (2011) consider force balance on Jakobshavn Isbræ at three different times (1995, 2000, and 2005) to evaluate changes in location and magnitude of flow resistance that accompanied the doubling of ice discharge and the contemporaneous surface lowering. They propose the rapid changes on this major outlet glacier resulted from weakening of the lateral shear margins; but without additional observations, the available measurements of surface speed and geometry alone are insufficient to identify the actual physical processes responsible for the observed changes in partitioning of flow resistance.